

Multifractal wave functions of simple quantum maps

John Martin¹, Ignacio García-Mata², Olivier Giraud^{3,4,5} and Bertrand Georgeot^{3,4}

¹ *Institut de Physique Nucléaire, Atomique et de Spectroscopie,
Université de Liège, Bât. B15, B - 4000 Liège, Belgium*

² *Departamento de Física, Lab. TANDAR, Comisión Nacional de Energía Atómica,
Av. del Libertador 8250, C1429BNP Buenos Aires, Argentina*

³ *Université de Toulouse; UPS; Laboratoire de Physique Théorique (IRSAMC); F-31062 Toulouse, France*

⁴ *CNRS; LPT (IRSAMC); F-31062 Toulouse, France*

⁵ *LPTMS, CNRS and Université Paris-Sud, UMR 8626, Bât. 100, 91405 Orsay, France*

(Dated: July 8, 2010)

We study numerically multifractal properties of two models of one-dimensional quantum maps, a map with pseudointegrable dynamics and intermediate spectral statistics, and a map with an Anderson-like transition recently implemented with cold atoms. Using extensive numerical simulations, we compute the multifractal exponents of quantum wave functions and study their properties, with the help of two different numerical methods used for classical multifractal systems (box-counting method and wavelet method). We compare the results of the two methods over a wide range of values. We show that the wave functions of the Anderson map display a multifractal behavior similar to eigenfunctions of the three-dimensional Anderson transition but of a weaker type. Wave functions of the intermediate map share some common properties with eigenfunctions at the Anderson transition (two sets of multifractal exponents, with similar asymptotic behavior), but other properties are markedly different (large linear regime for multifractal exponents even for strong multifractality, different distributions of moments of wave functions, absence of symmetry of the exponents). Our results thus indicate that the intermediate map presents original properties, different from certain characteristics of the Anderson transition derived from the nonlinear sigma model. We also discuss the importance of finite-size effects.

PACS numbers: 05.45.Df, 05.45.Mt, 71.30.+h, 05.40.-a

I. INTRODUCTION

Multifractal behavior has been observed in a wide variety of physical systems, from turbulence [1] to the stock market [2] and cloud images [3]. It has been recognized recently that such a behavior can also be visible in quantum wave functions of certain systems. In particular, wave functions in the Anderson model of electrons in a disordered potential are multifractal at the metal-insulator transition (see e.g. [4–6]). Similar behaviors were seen in quantum Hall transitions [7] and in Random Matrix models such as the Power law Random Banded Matrix model (PRBM) [8, 9] and ultrametric random matrices [10]. Such properties have also been seen in diffractive systems [11] and pseudointegrable models, for which there are constants of motion, but where the dynamics takes place in surfaces more complicated than the invariant tori of integrable systems [12]. In all these models, this behavior of wave functions came with a specific type of spectral statistics, intermediate between the Wigner distribution typical of chaotic systems and the Poisson distribution characteristic of integrable systems [12, 13]. Recently, a new model of one-dimensional quantum “intermediate map” which displays multifractal behavior was proposed [14], and a version with random phases was shown semi-rigorously to display intermediate statistics [15]. This model is especially simple to handle numerically and analytically, and displays different regimes of multifractality depending on a parameter [16]. In parallel, new experiments allowed recently to observe the

Anderson transition with cold atoms in an optical potential [17, 18] using a one-dimensional “Anderson map” proposed in [19].

Although much progress has been made in the study of these peculiar types of systems, several important questions related to multifractality remain unanswered. In particular, many results were derived or conjectured in the framework of the Anderson model, and their applicability to other families of systems is not known. Also, the precise link between the multifractal properties of wave functions and the spectral statistics is not elucidated.

In order to shed some light on these questions, we systematically investigate several properties of the wave functions of the intermediate quantum map of [14, 15], and compare them to results obtained for the Anderson map. In these one-dimensional systems, wave functions of very large vector sizes can be obtained and averaged over many realizations. This enables to control the errors and evaluate the reliability of standard methods used in multifractal analysis. This also allows to check and discuss several important conjectures put forth in the context of Anderson transitions. Our results also enable to study the road to asymptotic behavior in such models, giving hints on which quantities are more prone to finite-size effects or can be visible only with a very large number of random realizations.

The manuscript is organized as follows. In Section II, we review the known facts and conjectures about quantum multifractal systems, which were mainly put forth in the context of the Anderson transition. In Section III, we

present the models that will be studied throughout the paper. Section IV discusses the numerical methods used in order to extract multifractal properties of the models. Section V presents the results of numerical simulations, allowing first to compare the different numerical methods of Section IV, and then to test the conjectures and results developed in the context of the Anderson transition to the two families of models at hand.

II. EARLIER RESULTS AND CONJECTURES

We first recall some basic facts about multifractal analysis. Localization properties of wave functions of components ψ_i , $i = 1, \dots, N$, in a Hilbert space of dimension N , can be analyzed by means of their moments

$$P_q = \sum_{i=1}^N |\psi_i|^{2q}. \quad (1)$$

The asymptotic behavior of the moments (1) for large N is governed by a set of multifractal exponents τ_q defined by $P_q \propto N^{-\tau_q}$, or by the associated set of multifractal dimensions $D_q = \tau_q/(q-1)$. Equivalently, the singularity spectrum $f(\alpha)$ characterizes the fractal dimensions of the set of points i where the weights $|\psi_i|^2$ scale as $N^{-\alpha}$. It is related to the multifractal exponents τ_q by a Legendre transform

$$f(\alpha) = \min_q (q\alpha - \tau_q). \quad (2)$$

Compared to classical multifractal analysis, the quantum wave functions in Hilbert space of increasing dimensions are considered as the same distribution at smaller and smaller scales. This allows to define properly the multifractality of quantum wave functions, although at a given dimension they correspond to a finite vector.

In many physical instances, only a single realization of the wave function is considered. However, as soon as several realizations are considered, as is the case in presence of disorder, the moments (1) are distributed according to a certain probability distribution, and multifractal exponents depend on the way ensemble averages are performed, and in particular on the treatment of the tail of the moments distribution. If the tail decreases exponentially or even algebraically with a large exponent, the two averages should give the same answer. On the other hand, if the moments decrease according to a power-law with a small exponent, the average $\langle P_q \rangle$ will be dominated by rare wave functions with much larger moments (whose magnitude directly depends on the number of eigenvectors considered), while the quantity $P_q^{\text{typ}} = \exp(\ln P_q)$ will correspond to the typical value of the moment for the bulk of the wave functions considered. To each of these possible averaging procedures corresponds a set of multifractal exponents, defined

by

$$\langle P_q \rangle \propto N^{-\tau_q}, \quad \tau_q = D_q(q-1), \quad (3)$$

$$P_q^{\text{typ}} \propto N^{-\tau_q^{\text{typ}}}, \quad \tau_q^{\text{typ}} = D_q^{\text{typ}}(q-1). \quad (4)$$

As soon as averages over several realizations are made there can be a discrepancy between τ_q and τ_q^{typ} . Historically this effect was seen in the context of the Anderson transition [6, 21] and was very recently confirmed by the analytical calculations of [22, 23] in the same model. More specifically, it was shown that the distribution of the normalized moments $y_q = P_q/P_q^{\text{typ}}$ is asymptotically independent of N and has a power-law tail

$$\mathcal{P}(y_q) \sim \frac{1}{y_q^{1+x_q}} \quad (5)$$

for large y_q [21, 24]. The multifractal exponents τ_q and τ_q^{typ} only coincide over an interval $[q_-, q_+]$ where $x_q > 1$. In the case of heavy tails $x_q < 1$, the averages $\langle P_q \rangle$ and $\exp(\ln P_q)$ yield different exponents.

This phenomenon has a counterpart in the singularity spectra $f(\alpha)$ and $f^{\text{typ}}(\alpha)$. While $f^{\text{typ}}(\alpha)$ cannot take values below 0 and terminates at points α_{\pm} such that $f^{\text{typ}}(\alpha_{\pm}) = 0$, the singularity spectrum $f(\alpha)$ continues below zero. The two spectra coincide over the interval $[\alpha_+, \alpha_-]$. It can be shown that outside the interval $[q_-, q_+]$ the set of exponents τ_q^{typ} are given by the linear relation $\tau_q^{\text{typ}} = q\alpha_+$ for $q > q_+$ and $\tau_q^{\text{typ}} = q\alpha_-$ for $q < q_-$ [6].

In [21], it was stated that the exponents τ_q and τ_q^{typ} can be related through the following relation which depends on the tail exponent of the moments distribution x_q :

$$x_q \tau_q^{\text{typ}} = \tau_q x_q. \quad (6)$$

Equation (6) was analytically proven for PRBM [8] for integer values of x_q and also in the limit of large bands for $q > 1/2$. It remains unclear to which extent Eq. (6) is valid for other types of systems. A consequence of the identity (6) for $q > q_+$ is that $x_q = q_+/q$. In the regime of weak multifractality where D_q is a linear function, the identity (6) implies that $x_q = (q_+/q)^2$ for $q_- < q < q_+$ [6, 8](see Subsection V.E. for details).

Finally, a further relation that we wish to investigate in the present paper has been predicted based on the nonlinear sigma model and observed in the 3D Anderson model at criticality and several other systems. It is a symmetry relation of multifractal exponents [25], which can be expressed as

$$\Delta_q = \Delta_{1-q}, \quad (7)$$

with $\Delta_q = \tau_q - q + 1$. For the singularity spectrum it gives $f(2-\alpha) = f(\alpha) + 1 - \alpha$.

The validity of these different relations will be investigated on two particularly simple models of quantum maps that we describe in the next section.

III. MODELS

A. Intermediate map

The properties of section II have been first observed for wave functions in the 3D Anderson model at criticality. In the present paper the first model we will consider is a quantum map whose eigenfunctions display similar multifractal properties in momentum representation. It corresponds to a quantization of a classical map, defined on the torus by

$$\bar{p} = p + \gamma \pmod{1}; \quad \bar{q} = q + 2\bar{p} \pmod{1}, \quad (8)$$

where p is the momentum variable and q the angle variable, while \bar{p} and \bar{q} are the same quantities after one iteration of the map. The corresponding quantum evolution can be expressed as

$$\bar{\psi} = \hat{U}\psi = e^{-2i\pi\bar{p}^2/N} e^{2i\pi\gamma\bar{q}}\psi \quad (9)$$

in operator notation, or equivalently as a $N \times N$ matrix in momentum representation:

$$U_{kk'} = \frac{\exp(-2i\pi k^2/N)}{N} \frac{1 - \exp(2i\pi N\gamma)}{1 - \exp(2i\pi(k - k' + N\gamma)/N)}, \quad (10)$$

with $0 \leq k, k' \leq N - 1$ [14]. For generic irrational γ , the spectral statistics of \hat{U} are expected to follow Random Matrix Theory. When γ is a rational number, $\gamma = a/b$ with a, b integers, spectral statistics are of intermediate type and eigenvectors of the map display multifractal properties. In order to study the effect of ensemble averaging on multifractal exponents, we will consider a random version introduced in [15], where the phases $2\pi k^2/N$ are replaced by independent random phases ϕ_k . We will also present numerical results obtained for the initial map given by (10).

B. Anderson map

An important system where multifractal wave functions have been observed corresponds to electrons in a disordered potential in dimension three. Indeed, the Anderson model [6] which describes such a situation displays a transition between a localized phase (exponentially localized wave functions) and a diffusive phase (ergodic wave functions) for a critical strength of disorder. At the transition point, the wave functions display multifractal properties [6] and the spectral statistics are of the intermediate type [26]. In order to compare this type of system with the previous one, we have studied a one-dimensional system with incommensurate frequencies, which has been shown to display an Anderson-like transition [19]. In [17] it was shown that it can be implemented with cold atoms in an optical lattice, which enables to probe experimentally the Anderson transition.

The system is a generalization of the quantum kicked rotator model, and is described by a unitary operator which evolves the system over one time interval:

$$\bar{\psi} = \hat{U}\psi = e^{-iV(\hat{\theta}, t)} e^{-iH_0(\hat{n})}\psi, \quad (11)$$

with $V(\hat{\theta}, t) = k(1 + \epsilon \cos \omega_1 t \cos \omega_2 t) \cos \hat{\theta}$ (here time t corresponds to number of kicks). Here ω_1 and ω_2 should be two frequencies mutually incommensurate. Following [17] we chose in the simulations $\epsilon = 0.75$, $\omega_1 = 2\pi\lambda^{-1}$ and $\omega_2 = 2\pi\lambda^{-2}$, where $\lambda = 1.3247\dots$ is the real root of the cubic equation $x^3 - x - 1 = 0$. In [19] it was shown that this system displays an Anderson-like transition at the critical value $k_c \approx 1.81$, but multifractality of this system was up to now not verified. The function $H_0(n)$ can be chosen either by taking $H_0(n) = n^2/2$ (free evolution) or as in the preceding case by replacing this quantity by independent random phases uniformly distributed in the interval $[0, 2\pi[$. This is actually what we chose to do in our numerical simulations, in order to increase the stability and accuracy of the numerical results.

As a wave packet spreads slowly at the transition, one has to iterate the map for a long time in order to obtain data on a sufficiently large wave function. We found that in order to reach vector sizes of order 2^{11} , it was necessary to iterate the map up to $t = 10^8$. Such values are not realistic for experiments with cold atoms (limited to a few hundreds kicks) but allow to obtain more precise results.

C. Variations on the models

In both models the evolution of the system during one time step has the form of an operator diagonal in momentum (kinetic term) times an operator diagonal in position (kick term). In both cases, it has been common practice in the field to replace the kinetic term by random phases. This allows to obtain a similar dynamics but with a more generic behavior. Moreover, it enables averages over random phases to be performed, which makes numerical and analytical studies more precise. In contrast, in experiments with cold atoms it is easier to perform iterations with a true kinetic term rather than with random phases. In order to assess the effect of this modification, we will therefore use both approaches in the study of multifractal properties of wave functions.

Many works on multifractal wave functions have focused on eigenstates of the Hamiltonian (see e.g. [6]). For the intermediate map, the evolution operator has eigenvectors which can be numerically found and explored. It is also possible to evolve wave packets, for example initially concentrated on one momentum state, and to study the multifractality of the wave packet as time increases. This corresponds more closely to what can be explored in experiments. For the intermediate map, this process can be understood as the dynamics of a superposition of eigenvectors of the evolution operator. However, in the case of the Anderson map, the evolution operator is time

dependent (the continuous time problem being not periodic), and the connection with eigenvectors is lacking. In the following, we will explore and compare the multifractality of both eigenfunctions and time-evolved wave packets for the intermediate map.

IV. NUMERICAL METHODS

As is well-known, the numerical estimation of multifractal dimensions is very sensitive to finite-size effects. In the present work we have analyzed and compared different numerical methods in order to compute accurately the multifractal exponents. In this section we briefly review the methods we used.

A. Box-counting method

The most straightforward method is to compute directly the moments of the wave functions through the scaling of the moments (1) given by $P_q = \sum_i |\psi_i|^{2q}$. If the scaling (3) holds true, then $\log\langle P_q \rangle$ is a linear function of $\log N$ and its slopes yield the exponents τ_q . For $q < 0$, coarse-graining over neighboring sites is necessary in order to avoid instabilities due to very small values of $|\psi_i|$.

A variation of the moment method is the box-counting method. It consists in taking a vector of fixed size N and summing the $|\psi_i|^2$ over boxes of increasing length. If $N = 2^n$, then we define

$$P_{q,k} = \sum_{i=0}^{2^{n-k}-1} \left(\sum_{j=0}^{2^k-1} |\psi_{i2^k+j}|^2 \right)^q \quad (12)$$

which corresponds to averaging the measure over boxes of length 2^k , $0 \leq k \leq n$. Starting from $k = 2$ allows to smooth out exceedingly tiny values of $|\psi_i|^2$ which otherwise yield non-accurate estimates of D_q for negative q . The two methods above give similar results, as was also carefully checked for the Anderson model in [20]. We will therefore in the following present results using the box-counting method to assess the properties of this type of procedures.

B. Wavelet transform method

Recently, alternative procedures to compute the multifractal spectrum based on the wavelet transform were developed [27]. The wavelets form a basis of functions as does the Fourier basis and a function expressed in this new basis gives the wavelet transform (WT). Unlike the Fourier basis wavelets are localized both in position and in momentum space (or time and frequency space). They are therefore suitable to probe the local variations of a function at different scales. They have become an essential tool for image and sound processing and compression.

A wavelet basis is constructed from a single function g called analyzing or mother wavelet. The rest of the basis is constructed by translations and compressions (expansions) of the analyzing wavelet g . The translations define a space variable while the compressions define the scale at which the function is analyzed. We define the WT of a (real) function h as

$$T_h(A, B) = \frac{1}{A} \int dx h(x) g\left(\frac{x-B}{A}\right), \quad (13)$$

where A is the scale variable and B is the space variable. As a consequence, $T_h(A, B)$ can be interpreted as a measure of how close the function h is to the mother wavelet at point B and at scale A .

The τ_q can be extracted from the WT in the following way. We define the partition function

$$\mathcal{Z}(q, A) = \sum_{B_i} |T_h(A, B_i)|^q, \quad (14)$$

where $(A, B_i)_i$ are the local maxima at scale size A and q is real. It can be shown that τ_q appears as the exponent in the power law behavior of $\mathcal{Z}(q, A)$

$$\mathcal{Z}(q, A) \underset{A \rightarrow 0^+}{\sim} A^{\tau_q}. \quad (15)$$

This is essentially the method known as wavelet transform modulus maxima (WTMM) [27]. This method is developed for continuous wavelet function.

If the function h is sampled as an N -dimensional vector with $N = 2^n$ the wavelet transform can be discretized and implemented efficiently by a hierarchical algorithm [28] resulting in a fast wavelet transform, (FWT). The scale and space parameters take the values

$$A = 1, \frac{1}{2}, \frac{1}{4}, \dots, \frac{1}{2^{n-1}} \quad (16)$$

$$B_A \in \left\{ 1, 2, \dots, \frac{1}{A} \right\} \quad (17)$$

respectively. Starting from a wave function ψ and using a proper normalization at each scale, we redefine the partition function as

$$\mathcal{Z}(q, A) = \sum_{B_i} \left[\frac{|T_{|\psi|^2}(A, B_i)|}{\sum_{B_i} |T_{|\psi|^2}(A, B_i)|} \right]^q \quad (18)$$

where again $(A, B_i)_i$ are the local maxima at scale A . As in the continuous case $\mathcal{Z}(q, A)$ exhibits the same power law behavior as Eq. (15). In the following, we will present results using this implementation of the wavelet method, using the Daubechies 4 mother wavelet [29].

We note that, although the partition function (18) is the most standard, recently it was numerically observed [30] that for a complex multifractal wave function ψ , the exponents τ_q can also be obtained from the power law behavior of a modified partition function defined from the complex FWT of ψ and using $2q$ as exponents in Eq. (18).

V. RESULTS

A. Numerical computation of the multifractal exponents

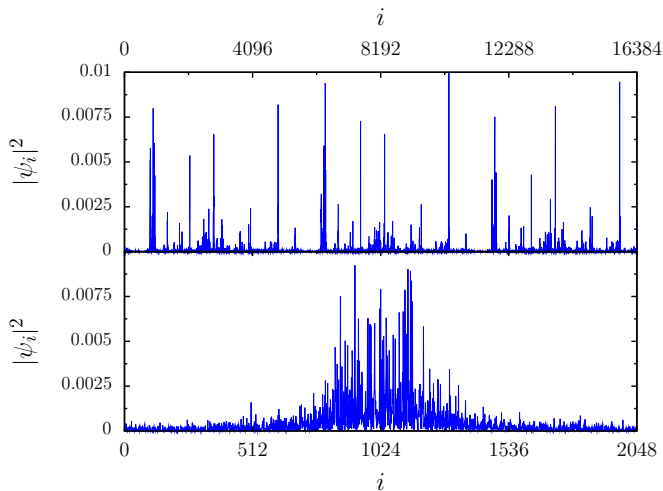


FIG. 1: (Color online) Top panel: Instance of an eigenvector of the intermediate map with random phases for $N = 2^{14}$ and $\gamma = 1/3$. Bottom panel: Instance of an iterate of the Anderson map with random phases for $k = 1.81$, $N = 2^{11}$ and $t = 10^8$; $|\psi(0)\rangle = |i\rangle$ with $i = 1024$.

In this subsection, we present numerical results corresponding to the multifractal exponents for the intermediate quantum map model (10) and the Anderson map (11). Examples of wave functions for both models are shown in Fig. 1. The two sets of multifractal dimensions D_q and D_q^{typ} were computed from $\log_2 \langle P_{q,k} \rangle$ and $\langle \log_2 P_{q,k} \rangle$ respectively for the box-counting method, and from $\log_2 \langle \mathcal{Z}(q, A) \rangle$ and $\langle \log_2 \mathcal{Z}(q, A) \rangle$ respectively for the wavelet method. For the Anderson map, as less realizations of the random phases could be computed, the same set of random realizations were used for the two methods investigated in order to ensure that comparable quantities were plotted. Figure 2 illustrates the scaling of these quantities for the two models considered. It displays $\log_2 \langle P_{q,k} \rangle$ as a function of the logarithm of the box size (top) and $\log_2 \langle \mathcal{Z}(q, A) \rangle$ as a function of the logarithm of the scale parameter $\log_2 A$ (bottom) for different values of q . We chose to show the scaling of these moments since it is the worst case, the curves for $\langle \log_2 P_{q,k} \rangle$ and $\langle \log_2 \mathcal{Z}(q, A) \rangle$ being always closer to linear functions. Nevertheless, Fig. 2 shows that the scaling is indeed linear over several orders of magnitude. The slopes of the linear fits give the multifractal exponents. In the two methods, there is a certain freedom in determining the range of box sizes (or scales for the wavelet method) over which the linear fit is made (the one we chose is indicated by the shaded area in Fig. 2). Usually for moderate values of q in absolute value, the result does not depend very much on this choice. As can be seen in Fig. 2, the

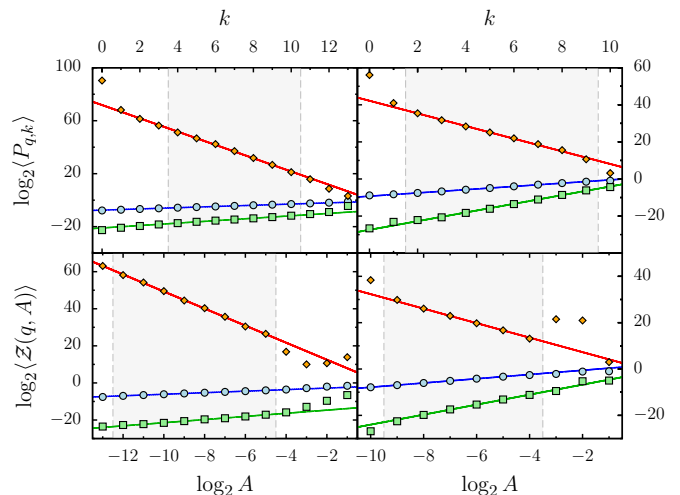


FIG. 2: (Color online) Top panels: Average moments $\log_2 \langle P_{q,k} \rangle$ as a function of k , the logarithm of the box sizes. Bottom panels: Partition function $\log_2 \langle \mathcal{Z}(q, A) \rangle$ as a function of the logarithm of the scale A . The left panels correspond to eigenvectors of the Intermediate map with random phases, $N = 2^{14}$, and $\gamma = 1/3$. Here the average is taken over 98304 vectors (resp. 32768 vectors for the partition function). The right panels correspond to iterates of the Anderson map for $k = 1.81$, $N = 2^{11}$, $|\psi(0)\rangle = |i\rangle$ with $i = 1024$ and $t = 10^8$, where the average is taken over 1302 vectors. The values chosen for q are : $q = -2$ (red diamonds), $q = 2$ (blue circles), and $q = 6$ (green squares). The gray shaded regions show the fitting interval.

data are well fitted by a linear function in the range chosen; however, there is still an uncertainty on the slope, which usually gets larger for large negative q . In the next figures of this subsection, the uncertainty of the linear fit for the set of points chosen is plotted together with the mean value, in order to give an estimate of the reliability of the values obtained.

The values of D_q and D_q^{typ} as a function of q are presented in Fig. 3 for the random intermediate map and in Fig. 4 for the Anderson map. In both cases, we observe a spectrum typical of multifractal wave functions. In the intermediate case, we observe that the two methods give comparable results with small uncertainty, although it gets larger for large negative q . For the Anderson map, the uncertainty gets very large for $q \lesssim -2$, and besides it begins to depend strongly on the range of box sizes (box-counting method) or scales (wavelet method) chosen (data not shown). We attribute the larger uncertainty for the wavelet method to the seemingly stronger sensitivity of this method to exceptionally small values. We note that for the Anderson map only a vector size of 2^{11} could be reached numerically because of the computational power required to iterate the Anderson map for long times. The discrepancy between the two methods is smaller for D_q^{typ} , which can be understood by the fact that $\langle P_{q,k} \rangle$ or $\langle \mathcal{Z}(q, A) \rangle$ are more sensitive to rare events than $\langle \log_2 P_{q,k} \rangle$ and $\langle \log_2 \mathcal{Z}(q, A) \rangle$.

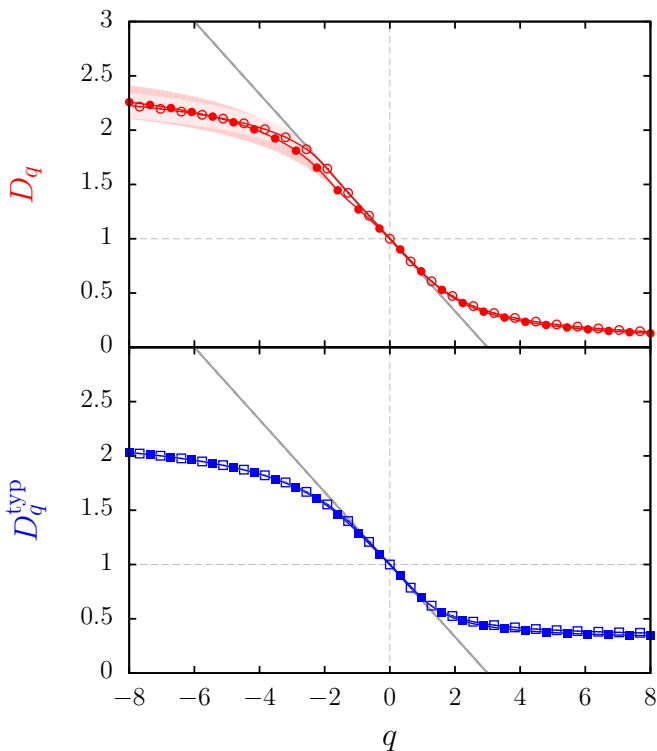


FIG. 3: (Color online) Top panel: Multifractal exponents D_q for eigenvectors of the Intermediate map with random phases, $N = 2^{14}$, and $\gamma = 1/3$. Empty/filled red circles correspond to the method of moments/wavelets. The (light blue, light red) shaded regions indicate standard error in the least squares fitting. The multifractal analysis was done over 98304 vectors with box sizes ranging from 16 to 1024 and scales ranging from 2 – 12 to 2 – 5. Bottom panel: Typical multifractal exponents D_q^{typ} for the same data. In both panels, the gray solid line is the linear approximation $1 - q/3$.

Our data nevertheless show that the iterates of the Anderson map display multifractal behavior. In view of the recent implementation of such maps with cold atoms [17], this indicates that in principle one can observe multifractality of this map in cold atom experiments; we note that in [18] properties of the wave functions of this experimental system were investigated, but focused on the envelope of the wave packet.

In both the intermediate map and the Anderson map, D_q^{typ} goes to a constant α_+ for large q , which corresponds to the fact already mentioned that τ_q^{typ} is expected to behave as $\tau_q^{\text{typ}} = q\alpha_+$ for $q > q_+$. This will be studied in more detail in the next section.

In [16] we observed the existence of a linear regime around $q = 0$, with slope $-1/b$ for the random intermediate map with parameter $\gamma = 1/b$. This regime seemed to be valid in quite a large interval around zero. The data displayed in Fig. 3 obtained by two different large-scale computations confirm this result, and show that this regime exists for both types of averages. We will

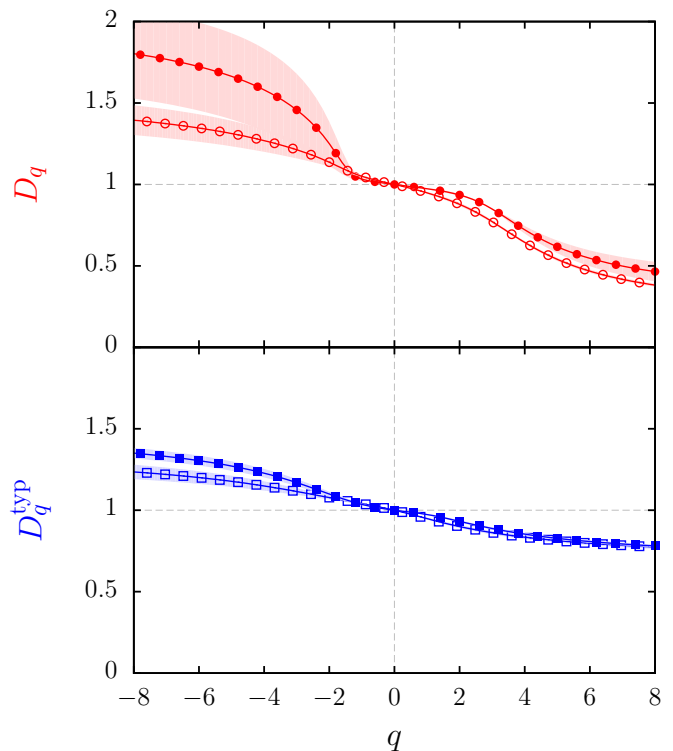


FIG. 4: (Color online) Multifractal exponents D_q and D_q^{typ} for iterates of the Anderson map with $k = 1.81$, $N = 2^{11}$. Same convention as in Fig. 3. The multifractal analysis was done over 1302 realizations of size $N = 2^{11}$ with box sizes ranging from 4 to 512 and scales ranging from 2 – 9 to 2 – 4.

come back to this property in section VB.

The data presented in Fig. 4 show that the Anderson vectors are less fractal than the eigenvectors of the intermediate map for $b = 3$. This can be expected from the fact that Anderson vectors correspond to iterates of a quantum map, which in general are less fractal than eigenvectors [31]. In order to compare similar quantities, we display in Fig. 5 multifractal dimensions for vectors obtained by iteration of the intermediate map for $b = 3$. One sees that using iterates instead of eigenvectors also in this case reduces the overall multifractality at a given q . Although a simple relation between multifractal exponents of eigenvectors and iterates is still lacking, this indicates that it might be possible to use experimental results from cold atom experiments to infer properties of the eigenvectors of the 3D Anderson transition.

In order to assess the effect of random phases, we present in Fig. 6 the results of numerical computation of D_q and D_q^{typ} for the intermediate map (10) without random phases. Although spectral statistics for random and non-random vectors are very close [15], the obtained fractal dimensions are quite different. Moreover it can be seen that there still exists a difference between D_q and D_q^{typ} , although the map is not random any more. The discrepancy in the two sets of exponents was to our

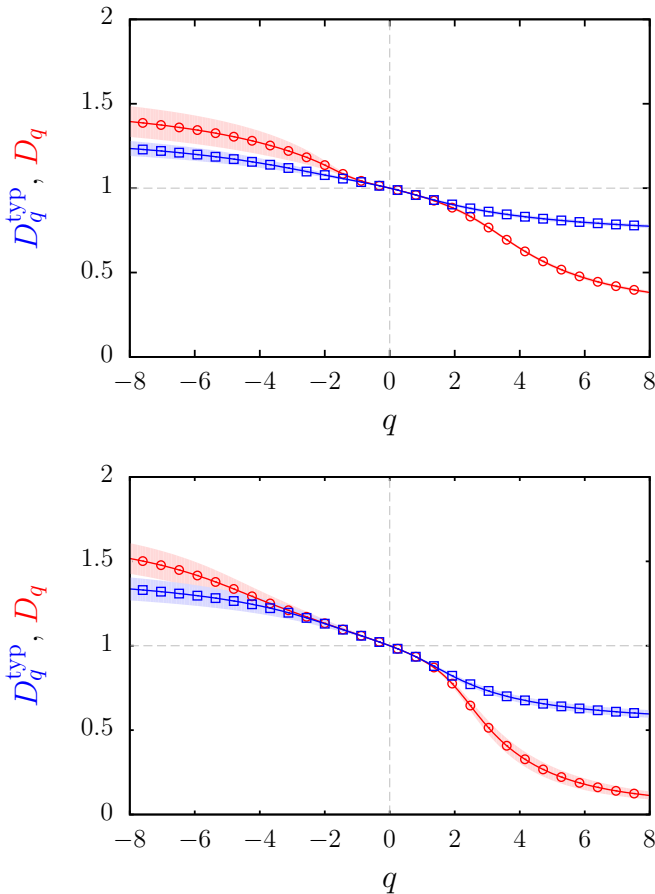


FIG. 5: (Color online) Top: Multifractal exponents D_q and D_q^{typ} for the Anderson map with $k = 1.81$, $N = 2^{11}$, $|\psi(0)\rangle = |i\rangle$ with $i = 1024$ and $t = 10^8$. Same convention as in Fig. 3. The multifractal analysis was done over 1302 realizations with box sizes ranging from 4 to 512. Bottom: Multifractal exponents D_q and D_q^{typ} for iterates of the intermediate map with $b = 3$, $N = 2^{12}$, $|\psi(0)\rangle = |i\rangle$ with $i = 2048$ and $t = 10^8$. The multifractal analysis was done over 2000 realizations with box sizes ranging from 4 to 512. In both cases we used the box-counting method.

knowledge up to date observed only in disordered systems, where rare events are created by specific realizations of disorder. It is interesting to see that this effect can be observed in a dynamical system without any disorder whatsoever. This discrepancy is due to the fact that the average in Eqs. (3)-(4) is performed over several eigenvectors of a single realization of the map, which gives a certain dispersion of the moment distribution. The average over eigenvectors in the intermediate map thus suffices to create the effect even in a deterministic map. Therefore one can also observe the separation between the two sets of exponents in quantum systems without disorder. The rare events in this case correspond to rare eigenvectors of the evolution operator having large moments.

The numerical results displayed in this Subsection in-

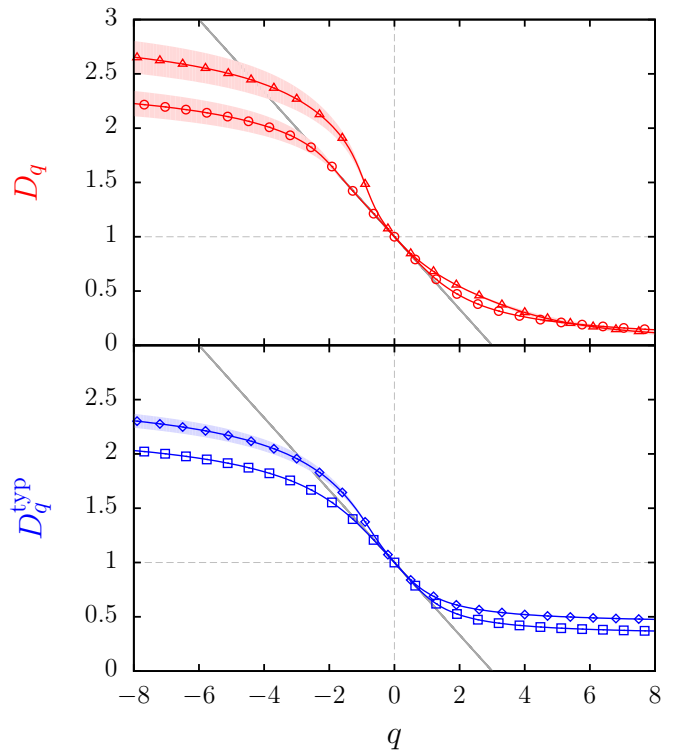


FIG. 6: (Color online) Top panel: Multifractal exponents D_q for eigenvectors of the intermediate map with (circles) and without (triangles) random phases. Bottom panel: Typical multifractal exponents D_q^{typ} for eigenvectors of the intermediate map with (squares) and without (diamonds) random phases. In both cases we used the box-counting method. Conventions and parameter values are the same as in Fig. 3 except that for non-random phases, a single realization of size $N = 2^{14}$ was considered. In both panels, the gray solid line is the linear approximation $1 - q/3$.

dedicate that multifractality is indeed present in all models considered. Furthermore, our results show that for an appropriate choice of a range of box sizes (box-counting method) or scales (wavelet method), both methods are based on curves well-fitted by linear function over a wide interval, with a small uncertainty on the exponent extracted. We believe that the good agreement for $q \gtrsim -2$ between the two methods, and the small uncertainty found for the linear fit, indicates that our numerically extracted multifractal exponents are reliable (up to finite size effects). For $q \lesssim -2$, the numerical uncertainty increases for decreasing q , and the two methods give increasingly different results. The results presented here show that our data are still reliable, although less precise, for eigenvectors of the intermediate map, even for negative q . However, in the case of the Anderson map, the uncertainty is too large to give reliable results for $q \lesssim -2$. This is certainly due to the fact that both the number of realizations and the vector sizes are smaller in this case, which makes it difficult to find reliable results in the more demanding regime of large negative q .

In the regime of $q \gtrsim -2$, our results indicate that the two methods can be used and give similar results. In the more demanding cases (large negative q) we found the box-counting method more reliable and accurate, and therefore the numerical results presented in the following Subsections correspond to this method.

B. Linear regime

In [16] the first investigations of the multifractal exponents for the random intermediate map showed the presence of a linear regime around $q = 0$ over a relatively large range of q values. We recall that the map (10) displays multifractal properties of rational values of the parameter $\gamma = a/b$. Based on semi-heuristic arguments, this linear regime was shown to be described by:

$$D_q \approx D_q^{\text{lin}} = 1 - \frac{q}{b}. \quad (19)$$

The relation (19) enables to link the spectral statistics and the distribution of D_q around $q = 0$ in a systematic way since both are controlled by the parameter b explicitly. While one expects that some form of linear regime should exist over small intervals for any smooth curve, the extent of it in this particular model indicated a small second derivative near $q = 0$. This feature was seen in the PRBM model [6] but in the regime of weak multifractality where the derivative at $q = 0$ of D_q is very close to zero.

Figure 7 displays the extent of the linear regime for the intermediate map for three values of the parameter $\gamma = 1/b$. The data presented show that the linear regime is present in all three cases, although its extent seems to be larger for large b (weak multifractality). This indicates that the linear regime is a robust feature of the random intermediate map. To explore more precisely the dependence of this regime on the value of b , the inset of Fig. 7 shows the separation point between the actual exponent and the linear value, defined by a constant relative difference (set to 1%), for all values of b between $b = 2$ and $b = 13$. The data presented show that indeed the extent of the linear regime grows with b , although the precise law of this growth is difficult to specify.

These results correspond to the random intermediate map, where the kinetic term is replaced by random phase. It is important to explore also the behavior of the deterministic intermediate map, where the kinetic term is kept as a function of momentum. In this case, Fig. 7 shows the presence of a much smaller linear regime. This indicates a strong difference between the random model and the deterministic one, and that a large linear regime is a property restricted to a certain kind of models.

The data for the Anderson map with random phases, shown in Fig. 8, also show a linear regime, comparable with the random intermediate map. Again, as the data correspond to iterates of wave packets, not eigenvectors, the multifractality is weaker than for other simulations

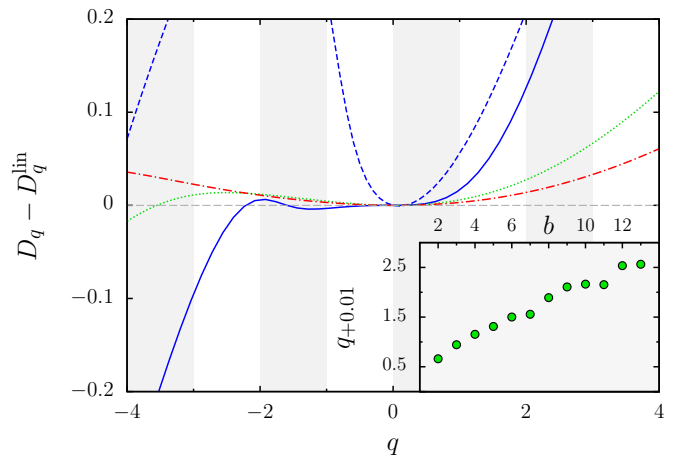


FIG. 7: (Color online) Difference $D_q - D_q^{\text{lin}}$ for eigenvectors of the intermediate map with random phases for $\gamma = 1/3$ (blue solid curve), $\gamma = 1/7$ (green dotted curve) and $\gamma = 1/11$ (red dash-dotted curve). Blue dashed curve shows the same difference for the intermediate map without random phases for $\gamma = 1/3$. Inset: separation points between D_q and D_q^{lin} (green dots), determined by $(D_q - D_q^{\text{lin}})/(D_q + D_q^{\text{lin}}) = 0.01$, for eigenvectors of the intermediate map with random phases for different values of $\gamma = 1/b$. Other parameters as in Fig. 6.

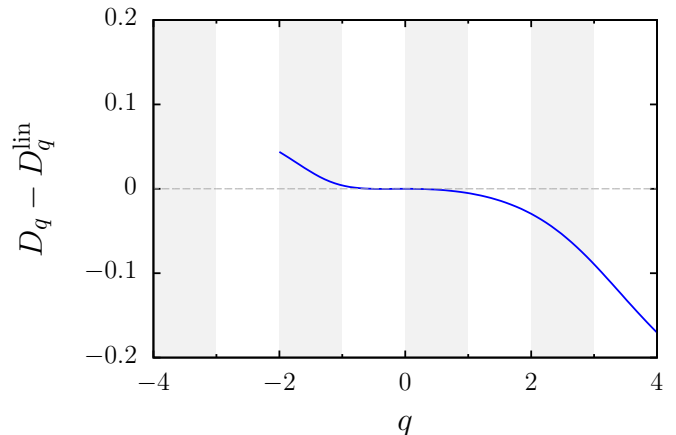


FIG. 8: (Color online) Difference $D_q - D_q^{\text{lin}}$ for iterates of the Anderson map, with D_q^{lin} defined by $D_q^{\text{lin}} = 1 + qD'_q(0)$. Same parameters as in Fig. 4.

of the Anderson model using eigenvectors [6]. This might explain why the linear regime that is visible seems larger than for Anderson transition eigenstates.

C. Average vs typical multifractal exponents

In disordered systems, the statistical distribution of the moments of the wave function is responsible for a discrepancy between the multifractal exponents D_q and D_q^{typ} calculated respectively by averaging over the mo-

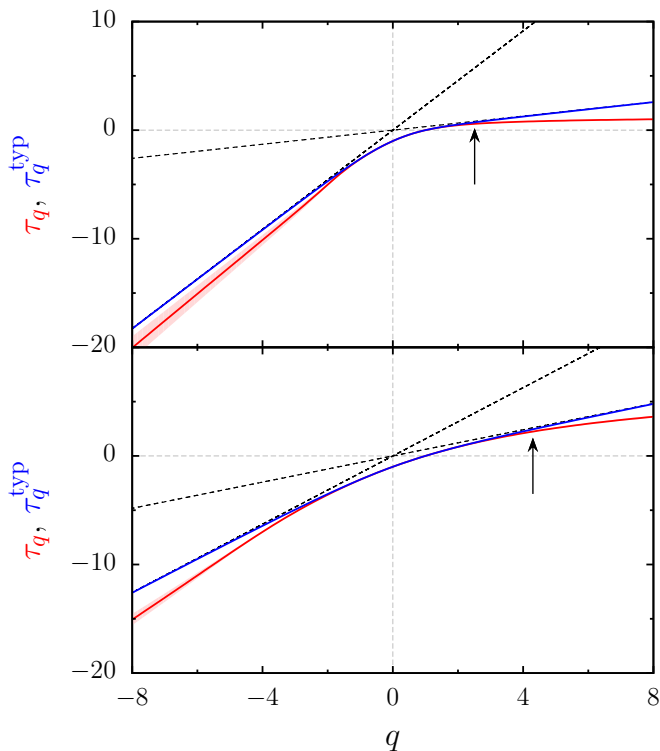


FIG. 9: (Color online) Top panel: Exponents τ_q (red solid lower curve) and τ_q^{typ} (blue solid upper curve) as a function of q for eigenvectors of the intermediate map with random phases, $N = 2^{14}$, and $\gamma = 1/3$. Bottom panel: same but for $\gamma = 1/11$. In both panels, the black dashed lines are linear fits of τ_q^{typ} at large $|q|$. The arrows indicate the critical q value determined by $x_q = 1$ (see Subsection V.D), equal to 2.51 for $\gamma = 1/3$ and to 4.30 for $\gamma = 1/11$. The slopes of the black dashed lines are respectively given by $\alpha_- \approx 2.28$ and $\alpha_+ \approx 0.32$ for $\gamma = 1/3$ and by $\alpha_- \approx 1.57$ and $\alpha_+ \approx 0.60$ for $\gamma = 1/11$.

ments themselves or over their logarithm. The two sets of exponents are expected to match only in some region $q \in [q_-, q_+]$. Outside this range, τ_q^{typ} should follow a linear behavior. Figure 9 displays results for τ_q and τ_q^{typ} for the intermediate map with parameter $\gamma = 1/b$ for two representative values of b . As expected from the PRBM model [6], in the case of weak multifractality ($\gamma = 1/11$, bottom panel of Fig. 9), the range over which the exponents are equal is wider than for strong multifractality ($\gamma = 1/3$, top panel of Fig. 9). Beyond that interval the behavior of τ_q^{typ} is linear for both values of γ . For positive q the linear tail appears around $q \simeq 2.5$ for $\gamma = 1/3$ and $q \simeq 4.3$ for $\gamma = 1/11$. The slopes of the linear tails give α_- and α_+ . According to the theory (see Section II), these values of α correspond to the terminating point of the singularity spectrum $f^{\text{typ}}(\alpha)$ defined in Eq. (2). We obtained comparable results for the Anderson map (data not shown).

In order to take a closer look at the discrepancy between the two sets of exponents, we plot the difference

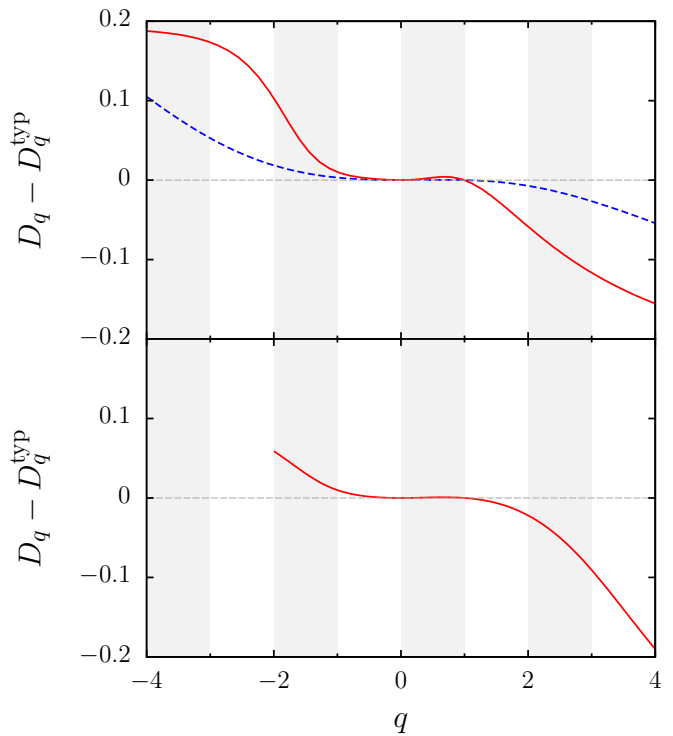


FIG. 10: (Color online) Top panel: Difference $D_q - D_q^{\text{typ}}$ between average and typical exponents for eigenvectors of the intermediate map with random phases for $\gamma = 1/3$ (red solid curve) and $\gamma = 1/11$ (blue dashed curve). Bottom panel: same figure for iterates of the Anderson map. Same parameters as in Fig. 4.

between the exponents D_q and D_q^{typ} for both systems. It is clearly seen in Fig. 10 that in all cases the regime where the exponents coincide is only about $-1 < q < 1$. At this scale the separation between τ_q and τ_q^{typ} occurs around $q = 1$. In order to obtain more systematically the separation point, we have plotted in Fig. 11 the value of q defined by a constant relative value of the difference of the two exponents (set equal to 0.01) for intermediate maps with different parameters $\gamma = 1/b$; this allows to get comparable data independently of the value of the exponents. The results show a clear linear scaling of the separation point with respect to b , obeying the formulas $q_{-0.01} + 1 \approx -0.1(b + 1)$ and $q_{+0.01} - 1 \approx 0.15(b - 1)$. Changing the threshold of relative value from 0.01 to 0.02 gives also a linear scaling, with different slope (data not shown).

The singularity spectrum $f(\alpha)$ defined in Eq. (2) is an alternative way to analyze multifractality and the discrepancy between the two sets of multifractal exponents. In Fig. 12 we show the singularity spectrum obtained for the intermediate map (10) with random phases (in [16] similar curves were obtained using directly the box-counting method to compute $f(\alpha)$; here we use the Legendre transform of the exponents, obtaining similar results). As expected $f^{\text{typ}}(\alpha)$ terminates at points α_+ and

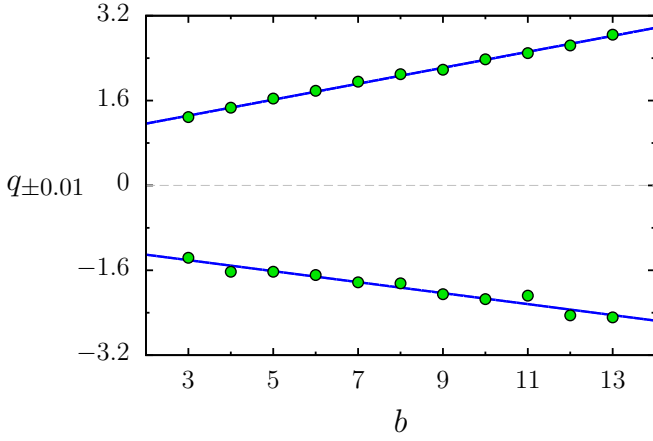


FIG. 11: (Color online) Separation points $q_{\pm 0.01}$ between D_q and D_q^{typ} (green dots), determined by $(D_q - D_q^{\text{typ}})/(D_q + D_q^{\text{typ}}) = \pm 0.01$, for eigenvectors of the intermediate map with random phases for different values of $\gamma = 1/b$. The blue solid lines are the linear fits $q_{-0.01} \approx -0.10b - 1.10$ and $q_{+0.01} \approx 0.15b + 0.86$. Same parameters as in Fig. 4.

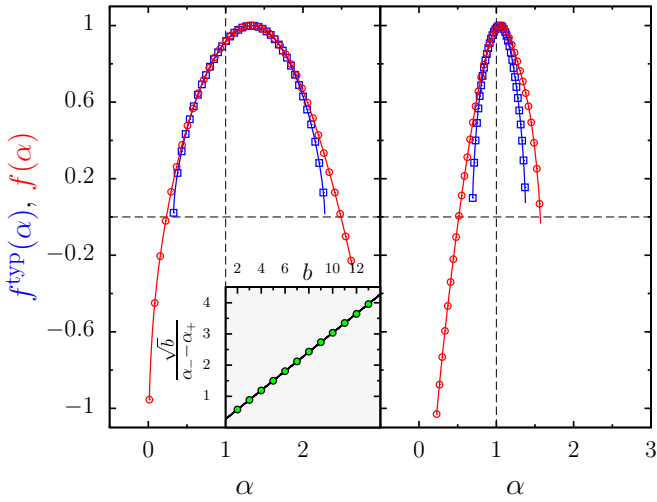


FIG. 12: (Color online) Left panel: Singularity spectra $f(\alpha)$ and $f^{\text{typ}}(\alpha)$ for eigenvectors of the intermediate map with random phases for $\gamma = 1/3$. The inset shows the linear behavior of $\sqrt{b}/(\alpha_- - \alpha_+) \simeq 0.307b - 0.037$ as a function of b (in $\gamma = 1/b$). The values of α_{\pm} have been extracted from linear fits of τ_q^{typ} at large $|q|$. Right panel: Singularity spectra $f(\alpha)$ and $f^{\text{typ}}(\alpha)$ for iterates of the Anderson map. In both panels, the singularity spectra are given in the range $\alpha(q = -16) \leq \alpha \leq \alpha(q = 16)$.

α_- given by the large- q slopes of τ_q^{typ} , while $f(\alpha)$ takes values below zero coming from statistically rare events. In [16], it was shown that a linear approximation for D_q yields a parabolic approximation for $f(\alpha)$, giving in turn a behavior $\alpha_- - \alpha_+ \simeq 1/\sqrt{b}$. We checked this behavior for all values of b between $b = 2$ and $b = 13$, thus confirming the validity of this law, even beyond the linear regime

(see inset of Fig. 12). Figure 12 allows a more direct comparison between multifractality in the intermediate map and the Anderson map: the narrower $f(\alpha)$ curve for Anderson corresponds to a weaker multifractality.

D. Moment distribution

The discrepancy between the two sets of multifractal exponents observed in the previous section is due to the fact that the moments P_q defined by (1) have a statistical distribution with a certain width. In particular for multifractal measures the distribution of the normalized moments $y_q = P_q/P_q^{\text{typ}}$ is expected to have a power-law tail at large q as $\mathcal{P}(y_q) \sim 1/y_q^{1+x_q}$, with an exponent x_q depending on q . In Fig. 13 we show an example of the

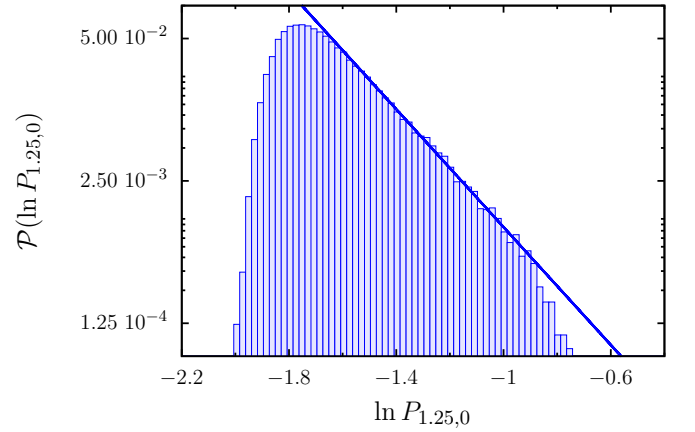


FIG. 13: (Color online) Probability distribution of the logarithm of the moment $P_q = P(q, 0)$ for $q = 1.25$ of eigenvectors of the random intermediate map for $\gamma = 1/3$. Same parameters as in Fig. 3. The solid line shows a linear fit (in log scale) whose slope yields the tail exponent $-x_q$.

distribution of the logarithm of the moments P_q for the random intermediate map. The distribution is indeed algebraic with a power law tail depending on q . While the linear behavior (in logarithmic scale) is clearly observed for small values of q (restricted to the range $q > 1$), this is not the case for larger q . We calculated the exponent x_q of the tail for a range of values of q where this exponent could be extracted. Results are displayed in Fig. 14 for the intermediate map and Fig. 15 for the Anderson map.

The value of q where $x_q \approx 1$ should correspond to the value q_+ where the two curves of D_q and D_q^{typ} (or τ_q and τ_q^{typ}) separate. As one can observe in Fig. 14 that value of q is rather difficult to estimate numerically with sufficient accuracy as the exponents x_q did not converge to a definite value at the largest vector size available ($N = 2^{14}$). However the curves seem to yield an exponent equal to 1 around $q \approx 2.51$ for $\gamma = 1/3$ and 4.3 for $\gamma = 1/11$. These values are indicated with black arrows in Fig. 9, and at that scale they do seem to coincide with points where τ_q

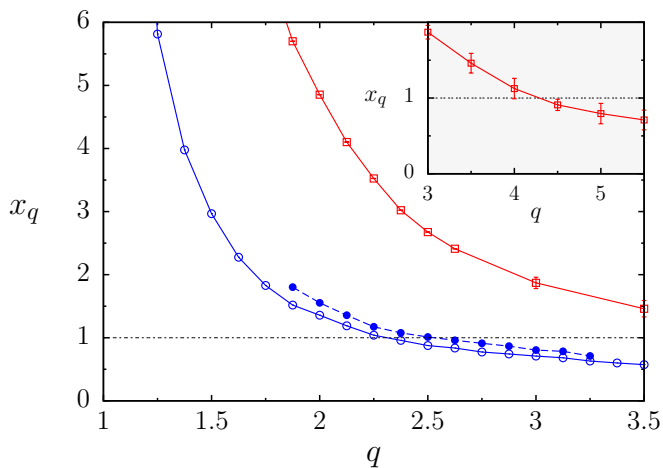


FIG. 14: (Color online) Tail exponents x_q for eigenvectors of the random intermediate map for $\gamma = 1/3$ with $N = 2^{12}$ (blue filled circles) and $N = 2^{14}$ (blue empty circles) and for $\gamma = 1/11$ with $N = 2^{14}$ (red squares). Same parameters as in Fig. 3. Inset: Tail exponent for $\gamma = 1/11$ for larger values of q .

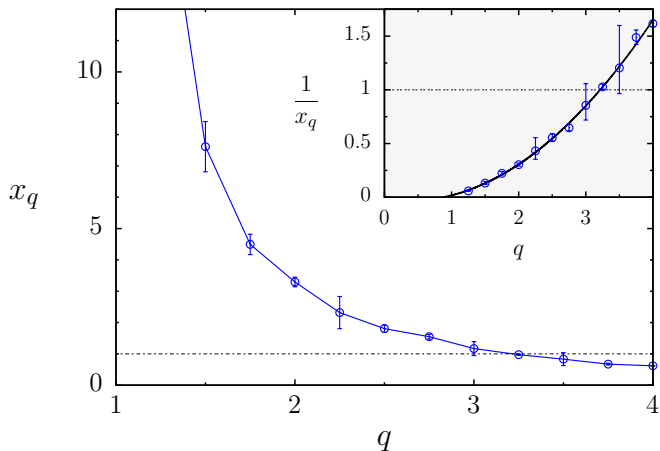


FIG. 15: (Color online) Tail exponents x_q for iterates of the Anderson map. Same parameters as in Fig. 4. The inset shows that $1/x_q$ is well-fitted by a parabola.

and τ_q^{typ} separate. However these points are far beyond the value $q \approx 1$ at which the multifractal dimensions D_q and D_q^{typ} separate at the scale of Fig. 10, and also different from the values obtained by fixing the relative difference of the exponents in Fig. 11 (equal to $q_{+0.01} = 1.31$ for $\gamma = 1/3$ and $q_{+0.01} = 2.51$ for $\gamma = 1/11$). The value where the curves separate is dominated by the rare events in the extreme tail of the distribution. The different values obtained indicate that indeed the numerical results are still far from the asymptotic regime. Similar conclusions can be drawn from Fig. 15, which presents the power-law tail exponents x_q obtained for the moment distribution of the Anderson vectors: the point where

$x_q = 1$ is reached around $q \approx 3$ while Fig. 10 seems to indicate a separation of the multifractal exponents around $q \approx 1$. We note that for the finite sizes considered, the value of x_q seems to become infinite as $q \rightarrow 1$, indicating that in this regime the distribution of moments is not any more fitted by a power law at large moments (see also Fig. 19). The behavior of the exponents x_q will be further discussed in the next Subsection.

E. Relation between multifractal exponents and moment distribution

As explained in Section II, it was proposed in [21] that the exponents τ_q and τ_q^{typ} were related to the moment distribution through the relation (6). This formula was proved only in some very specific cases, such as the PRBM model in the regime of weak multifractality, but conjectured to be generically valid. The results of the preceding subsections enable to check numerically whether this formula holds for our models.

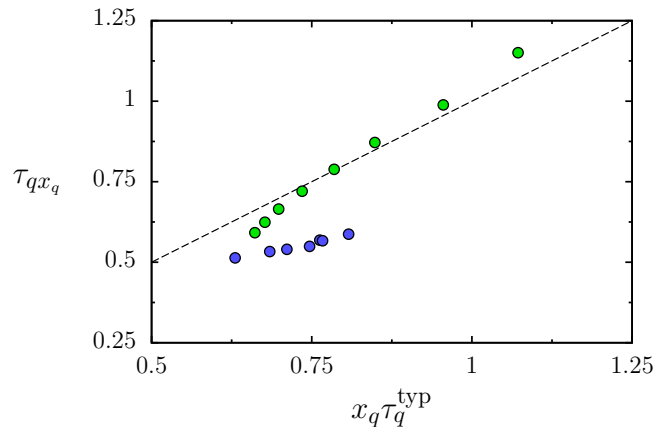


FIG. 16: (Color online) Relation between $\tau_q x_q$ and $x_q \tau_q^{\text{typ}}$ for eigenvectors of the intermediate map for $\gamma = 1/3$. Parameter values are the same as in Fig. 3. Blue/green (black/grey) circles correspond to values of q larger/smaller than 2.5 (the values closer to $q = 2.5$ are on the left for both series of points). Dashed line is the formula (6).

In Fig. 16,17 we show τ_{qx_q} as a function of $x_q \tau_q^{\text{typ}}$ for the random intermediate map with parameters $\gamma = 1/3$ and $\gamma = 1/11$. For $\gamma = 1/3$ (Fig. 16), it shows a certain agreement with the conjectured law for small values of q . Similarly for $\gamma = 1/11$ (Fig. 17) the agreement with the law (6) is good, but the actual slope seems slightly different. On the other hand, for $\gamma = 1/3$ and larger values of q the relation breaks down. We note that there is a certain ambiguity in the formula, since as can be seen in Fig. 16 one can have two values of τ_{qx_q} for the same value of $x_q \tau_q^{\text{typ}}$ (corresponding to two different values of q). The results indicate that the relation (6) can indeed be seen, even if approximately, in other systems that in Anderson transition models. Interestingly, the case $\gamma =$

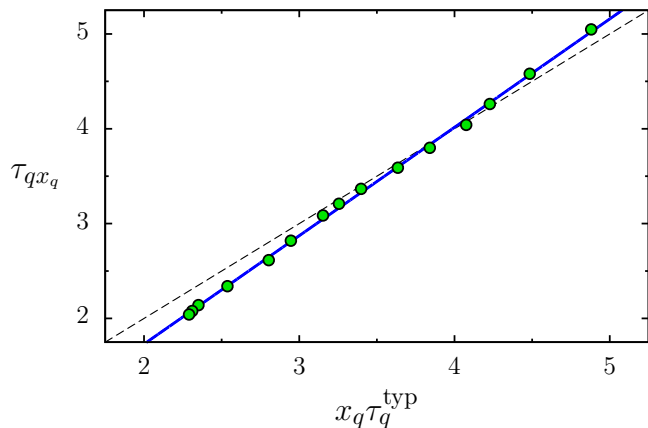


FIG. 17: (Color online) Relation between τ_{qx_q} and $x_q \tau_q^{\text{typ}}$ for eigenvectors of the intermediate map for $\gamma = 1/11$. Parameter values are the same as in Fig. 3. The blue solid line shows a linear fit of the data ($y = 1.14x - 0.56$). Dashed line is the formula (6).

$1/11$ corresponds to a case of weak multifractality. This might indicate that the relation is better verified in the case of weak multifractality, and only approximate in the general case. But we cannot exclude that the regime of weak multifractality leads to weaker finite-size effects and that the results for $\gamma = 1/3$ would eventually converge to the law (6) for larger sizes and many more realizations. An additional problem concerns the different scales of the two figures 16 and 17. As the multifractality is weaker in the case $\gamma = 1/11$, the values of x_q and τ_q are larger, leading to a much larger scale for the data in Fig. 17. It is possible that the finite-size effects are comparable but show more markedly in Fig. 16 due to its much smaller scale.

In Fig. 18 we present the same numerical analysis for the Anderson map. The results show that a linear law similar to (6) can be seen. The slope is close to one, but the curve is shifted by a relatively large offset (≈ 0.3). Note that the formula (6) was predicted for eigenvectors of the Anderson model and PRBM; here we are looking at iterates of wave packets, which can show different behavior.

Interesting properties of the exponents x_q can be deduced from the relation (6). As mentioned in the introduction, if such a relation is verified it implies that for $q > q_+$ (or equivalently $x_q < 1$) the inverse of the exponents x_q should follow a linear law. Indeed, for $q > q_+$ the exponent τ_q^{typ} is linear and one has $qx_q \alpha_+ = \tau_{qx_q} = D_{qx_q}(qx_q - 1)$, thus $z = qx_q$ is solution of the equation $D_z = \frac{z}{z-1} \alpha_+$. If this equation has an unique solution, then the quantity qx_q is a constant, equal to q_+ for $q = q_+$, and thus $1/x_q$ should be linear as a function of q for $q > q_+$. In order to check whether this holds in our case, we plot in Fig. 19 the values of $1/x_q$ as a function of q for the intermediate random map with parameters $\gamma = 1/3$ and $\gamma = 1/11$. In both cases,

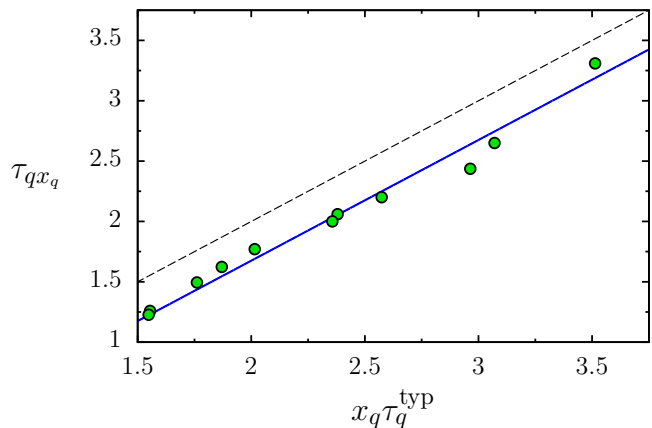


FIG. 18: (Color online) Relation between τ_q and τ_q^{typ} for iterates of the Anderson map with $k = 1.81$, $N = 2^{11}$, $|\psi(0)\rangle = |i\rangle$ with $i = 1024$ and $t = 10^8$. Parameter values are the same as in Fig. 4. The blue solid line correspond to $y = x - 0.29$. Dashed line is the formula (6).

a linear law agrees well with the data at large q , but obeys an equation different from the one predicted, with in particular an extra constant term which depends on γ .

A second consequence of relation (6) arises in the case where D_q is given by a linear function. This is in particular the case for the intermediate map in the regime of weak multifractality. In this regime it was observed [16] that for not too large q the multifractal exponents D_q are very closely given by the linear approximation $D_q = 1 - q/b$. Inserting this relation into (6), we get that for $q \in]q_-, q_+[$ (where D_q and D_q^{typ} are equal) the exponents are given by $x_q = b/q^2$ provided qx_q also belongs to $]q_-, q_+[$. We note that this in turn predicts a value $q_+ = \sqrt{b}$ for the separation point between the two sets of exponents, contrary to the linear scaling found in the data shown in Fig. 11. According to these considerations, in the small q regime and for weak multifractality, a quadratic behavior of $1/x_q$ should be observed provided the linear regime extends beyond the point q_+ . In the case $\gamma = 1/11$ for the intermediate map, the linear regime is verified quite far away from zero but breaks down before q_+ (see Fig. 10), thus D_{qx_q} is not a linear function of its argument. Still, Fig. 19 (lower panel) shows that the parabolic behavior of $1/x_q$ is retained for small values of q ; the inset shows that indeed a quadratic fit is much better than a linear fit in this range. In the strong multifractality regime, D_q is not linear any more beyond $q = 1$; in that case, the inset of the top panel in Fig. 19 shows that the behavior of $1/x_q$ is linear rather than quadratic.

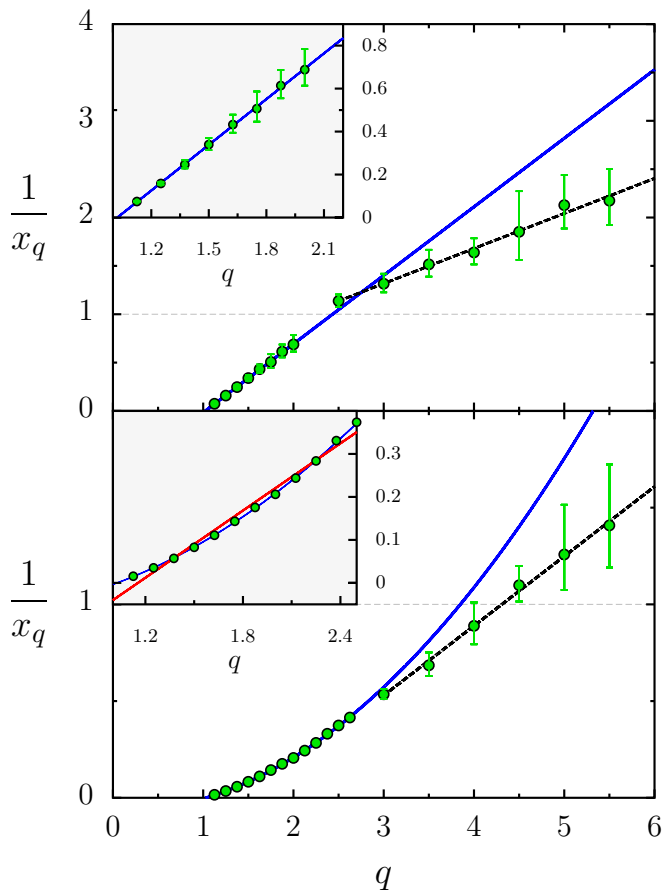


FIG. 19: (Color online) Inverse of the tail exponents x_q for eigenvectors of the random intermediate map. Top panel: $\gamma = 1/3$; blue and black dashed lines are linear fits in two different q range; dashed line (linear fit for large q) is $1/x_q = 0.36q + 0.23$; inset is a blow-up of the small q range. Bottom panel: $\gamma = 1/11$; blue and black dashed lines are respectively quadratic and linear fits in two different q range; dashed line (linear fit for large q) is $1/x_q = 0.36q - 0.55$; inset is a blow-up of the small q range, showing in red the best linear fit for the same data. In both cases, the two ends of the error bars correspond to two values of x_q obtained from a fit of the moments probability distribution over two different intervals. Parameter values are the same as in Fig. 3.

F. Symmetry between exponents

As described in Section II, it was predicted analytically and observed in the Anderson model at the transition that a symmetry exists between multifractal exponents. Indeed, the quantity $\Delta_q = \tau_q - q + 1$ follows the law $\Delta_q = \Delta_{1-q}$ (relation (7)). This relation was predicted on very general grounds, and expected to hold for all multifractal quantum systems. It was seen in the PRBM model [25], the Anderson model [20] and ultrametric random matrices [10]. It was also predicted to occur in simple multifractal cascade models in [23]. We performed systematic calculation of the quantity Δ_q for

each of the systems considered.

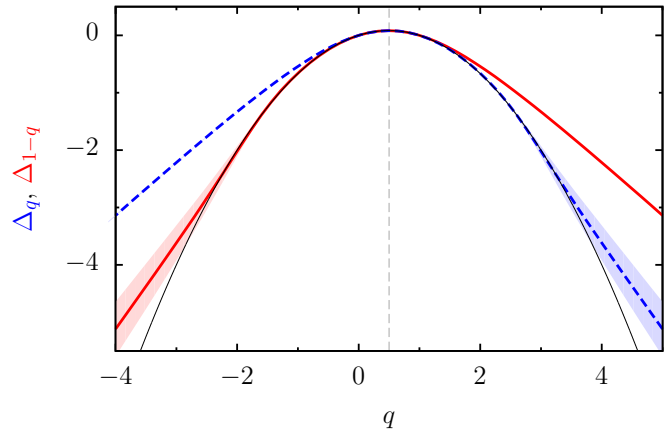


FIG. 20: (Color online) Anomalous exponents Δ_q (blue dashed curve) and Δ_{1-q} (red solid curve) for eigenvectors of the intermediate map with random phases, $\gamma = 1/3$ and $N = 2^{14}$. Parameter values are the same as in Fig. 3. The black thin line shows the parabola $q(1-q)/b$ corresponding to the linear regime.

Figure 20 shows the results of this analysis for the random intermediate map. The presence of a large linear regime complicates the picture, since the linear law described above in Subsection VB verifies the symmetry. Thus the intermediate map can show deviations from the symmetry only outside the linear regime. It turns out (comparing Figs. 7 and 20) that the symmetry (7) is only present in the linear regime and does not extend beyond its validity. This seems to indicate that the symmetry is absent from these models.

As the linear regime is much smaller in the case of the intermediate map without random phase, if the symmetry does not hold in this system we should expect a larger discrepancy in the nonrandom case. Fig. 21 displays Δ_q and Δ_{1-q} for the nonrandom intermediate case, showing that indeed the symmetry is verified in an even smaller range of q values than for the random case, in agreement with the small extent of the linear regime.

Finally, we have also computed the quantities Δ_q and Δ_{1-q} for iterates of the random intermediate map and of the random Anderson map. As said in Subsection V.A, the precision of the exponents degrades for $q \lesssim -2$ in the case of the Anderson map, so verification of the symmetry relation is delicate. Nevertheless, our results indicated that while for iterates of the random intermediate map the symmetry (7) still does not hold beyond the linear regime, in the case of the Anderson map the symmetry remains valid within the numerical error bars (which are however quite large) well beyond the linear regime (data not shown). This seems to indicate further that the symmetry is a feature of the Anderson model, which is clearly absent from the intermediate map.

Although we cannot prove rigorously that the symmetry relation (7) does not hold for intermediate systems,

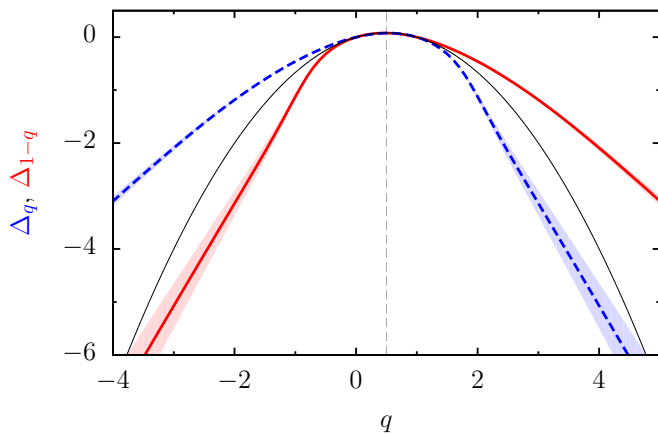


FIG. 21: (Color online) Anomalous exponents Δ_q (blue dashed curve) and Δ_{1-q} (red solid curve) for eigenvectors of the intermediate map (10) with $\gamma = 1/3$ and $N = 2^{14}$. The (light blue, light red) shaded region indicates standard error in the least squares fitting. The multifractal analysis was done with box sizes ranging from 16 to 1024. The black thin line shows the parabola $q(1-q)/b$ corresponding to the linear regime.

our results strongly indicate that it is violated in these systems as soon as the linear regime breaks down. To further confirm that our numerical method is able to observe the symmetry (7) in a system where it is present, we computed Δ_q and Δ_{1-q} for ultrametric random matrices where the relation is known to hold [10]. Our numerical method was able to confirm unambiguously the presence of the symmetry in this specific case (data not shown).

We note that in [25] the presence of the symmetry (7) for the Anderson transition was theoretically predicted on the basis of a renormalization group flow whose limit corresponds to a nonlinear sigma model. It would be interesting to see if a different nonlinear sigma model can apply to the intermediate map, or if it is the sign that these models cannot describe certain aspects of these systems.

VI. CONCLUSION

In this paper, we have studied the different multifractal exponents one can extract from the wave functions of the intermediate map and the Anderson map. Both models are one-dimensional, and thus allow much larger system size than the 3D Anderson transition, but in contrast to Random Matrix models such as the PRBM they correspond to physical systems with an underlying dynamics.

Our results enabled to extract the exponents over a large range of q values for the intermediate map. We have checked that two methods widely used in other contexts

(classical multifractal systems), namely the box-counting and the wavelet method, can be used to obtain reliably the exponents, giving similar results in most cases, although the box-counting method seems more robust for large negative values.

Our numerical data allow to confirm that the Anderson map introduced in [19] and experimentally implemented with cold atoms [17] indeed displays multifractal properties at the transition point, although this multifractality is weak. As concerns the intermediate map, our data confirm the existence of a linear regime for the multifractal exponents D_q and D_q^{typ} which was first seen in [16], well beyond the regime of weak multifractality. Interestingly enough, the linear regime is much smaller for the nonrandom intermediate map. We checked that the exponents D_q and D_q^{typ} are different also in the case of the intermediate map, even in the nonrandom case where no disorder is present.

Our numerical study of the moments of the wave functions and the multifractal exponents show that the generic behavior of D_q and D_q^{typ} predicted for the Anderson transition [6] are present for the Anderson map. Our results enable to extract the value of q_+ and q_- through the behavior of the moments of the wave functions together with the values of α_+ and α_- ; the fact that the value is different from the one obtained by direct computation of the multifractal exponents shows that finite size effects persist in such systems up to very large sizes. Note, however, that as our numerical computations correspond to very large system sizes, this might indicate that the asymptotic limit may be difficult to reach even in experimental situations. In addition, our investigations show that the relation (6) between the moments and the exponents conjectured in [21] is only approximately verified in our systems, even in the Anderson map. At last, the exact symmetry relation (7) between the multifractal exponents of the Anderson transition discovered in [25] is not present in intermediate systems.

Our results indicate that intermediate systems, and more generally quantum pseudointegrable systems, represent a type of model with some similarities with the Anderson transition model of condensed matter, but with specific properties. In particular, the absence of the symmetry present in the Anderson model between the exponents suggests proceeding with care in using the nonlinear sigma model to predict properties of these systems.

We think that further studies of these two kind of quantum systems are needed in order to elucidate the multifractal properties of quantum systems and their link with spectral statistics.

We thank E. Bogomolny, D. Delande, K. Frahm, C. Monthus and A. Ossipov for useful discussions. This work was supported in part by the Agence Nationale de la Recherche (ANR), project QPPRJCCQ and by a PEPS-PTI from the CNRS.

-
- [1] C. Meneveau, K. R. Sreenivasan, Phys. Rev. Lett. **59**, 1424 (1987); J.-F. Muzy, E. Bacry and A. Arneodo, Phys. Rev. Lett. **67**, 3515 (1991).
- [2] B. B. Mandelbrot, A. J. Fisher and L. E. Calvet, Cowles Foundation Discussion Paper No. 1164 (1997).
- [3] S. Lovejoy and D. Schertzer, Journal of Geophysical Research **95**, 2021 (1990).
- [4] A. D. Mirlin, Phys. Rep. **326**, 259 (2000).
- [5] E. Cuevas, M. Ortuno, V. Gasparian and A. Perez-Garrido, Phys. Rev. Lett. **88**, 016401 (2001).
- [6] F. Evers and A. D. Mirlin, Rev. Mod. Phys. **80**, 1355 (2008).
- [7] B. Huckestein, Rev. Mod. Phys. **67**, 357 (1995).
- [8] A. D. Mirlin, Y. V. Fyodorov, F.-M. Dittes, J. Quezada, and T. H. Seligman, Phys. Rev. E **54**, 3221 (1996).
- [9] V. E. Kravtsov and K. A. Muttalib, Phys. Rev. Lett. **79**, 1913 (1997).
- [10] Y. V. Fyodorov, A. Ossipov and A. Rodriguez, J. of Stat. Mech. **L12001** (2009).
- [11] A. M. Garcia-Garcia and J. Wang, Phys. Rev. E **73**, 036210 (2006).
- [12] E. B. Bogomolny, U. Gerland and C. Schmit, Phys. Rev. E **59**, R1315 (1999).
- [13] E. B. Bogomolny, O. Giraud and C. Schmit, Phys. Rev. E **65**, 056214 (2002).
- [14] O. Giraud, J. Marklof and S. O'Keefe, J. Phys. A **37**, L303 (2004).
- [15] E. B. Bogomolny and C. Schmit, Phys. Rev. Lett. **93**, 254102 (2004).
- [16] J. Martin, O. Giraud, and B. Georgeot, Phys. Rev. E **77**, 035201(R) (2008).
- [17] J. Chabé, G. Lemarié, B. Grémaud, D. Delande, P. Szriftgiser, and J.-C. Garreau, Phys. Rev. Lett. **101**, 255702 (2008); G. Lemarié, J. Chabé, P. Szriftgiser, J.-C. Garreau, B. Grémaud, and D. Delande, Phys. Rev. A **80**, 043626 (2009).
- [18] G. Lemarié, H. Lignier, D. Delande, P. Szriftgiser, and J.-C. Garreau (2010) preprint arXiv:1005.1540.
- [19] G. Casati, I. Guarneri, and D. L. Shepelyansky, Phys. Rev. Lett. **62**, 345 (1989).
- [20] L. J. Vasquez, A. Rodriguez and R. A. Römer, Phys. Rev. B **78**, 195106 (2008); A. Rodriguez, L. J. Vasquez and R. A. Römer, Phys. Rev. B **78**, 195107 (2008).
- [21] A. D. Mirlin and F. Evers, Phys. Rev. B **62**, 7920 (2000).
- [22] M. S. Foster, S. Ryu and A. W. W. Ludwig, Phys. Rev. B **80**, 075101 (2009).
- [23] C. Monthus and T. Garel, J. Stat. Mech. **2010**, P06014 (2010).
- [24] F. Evers and A. D. Mirlin, Phys. Rev. Lett. **84**, 3690 (2000).
- [25] A. D. Mirlin, Y. V. Fyodorov, A. Mildenberger and F. Evers, Phys. Rev. Lett. **97**, 046803 (2006).
- [26] B. I. Shklovskii, B. Shapiro, B. R. Sears, P. Lambrianides, and H. B. Shore, Phys. Rev. B **47**, 11487 (1993); D. Braun, G. Montambaux, and M. Pascaud, Phys. Rev. Lett. **81**, 1062 (1998).
- [27] A. Arneodo in *Wavelets: Theory and Applications*, G. Erlebacher, M. Y. Hussaini and L. M. Jameson, Eds (Oxford University Press, New York, 1996).
- [28] S. G. Mallat, IEEE Trans. on pattern analysis and machine intelligence, VOL. II, No 7, 674 (1989).
- [29] I. Daubechies, Comm. Pure Appl. Math. **41**, 909 (1988).
- [30] I. García-Mata, O. Giraud and B. Georgeot, Phys. Rev. A **79**, 052321 (2009).
- [31] O. Giraud and B. Georgeot, Phys. Rev. A **72**, 042312 (2005).